Finite-difference solution of the image wave equation for depth remigration: stability

Jörg Schleicher, Amélia Novais, and Fernando P. Munerato

email: *js@ime.unicamp.br*

keywords: *Seismic imaging, image waves, remigration*

ABSTRACT

The image wave equation for depth remigration is a partial differential equation that is similar to the acoustic wave equation. In this work, we determine the stability conditions that have to be met when solving the image wave equation by finite differences. The stability criterion exhibits a strong wavenumber dependence. Where higher horizontal than vertical wavenumbers are present in the data to be remigrated, stability may be difficult to achieve. Numerical tests demonstrate that the implementational form of the chosen FD scheme can be essential to obtain results with a limited numerical error even in situations where stability cannot be theoretically guaranteed.

INTRODUCTION

Seismic remigration is an imaging technique that envisages the construction of an improved migrated section for an updated macrovelocity model (e.g., one taking lateral velocity variations into account) on the basis of a previously migrated section as obtained with a different initial macrovelocity model (e.g., one employing simple velocity laws where the migration can be very efficiently realized). If the two macrovelocity models do not differ too much, one generally calls the imaging procedure that corrects the image a "residual migration" (Rothman et al., 1985). Where significant differences between both models are allowed, the process is referred to as remigration (Hubral et al., 1996a). In the seismic literature, it is also known as velocity continuation (Fomel, 1994).

The sequence of images of a certain reflector as subsequently migrated with varying migration velocities creates an impression of a propagating wavefront. This "propagating wavefront" was termed an "image wave" by Hubral et al. (1996b). The propagation variable, however, is not time as is the case for conventional physical waves as described, e.g., by the acoustic wave equation, but the migration velocity.

For homogeneous media, Hubral et al. (1996b) and Tygel et al. (1998) have studied the kinematic behaviour of these image waves as a function of the constant migration velocity. By treating them in a similar way as conventional acoustic waves, they derived partial differential equations that describe the "propagation" of the reflector image as a function of migration velocity for both, time and depth remigration. Therefore, these partial differential equations have been termed "image wave equations." Both image wave equations for time and depth remigration are equations similar to the acoustic wave equation (Fomel, 1994; Hubral et al., 1996b).

The image wave equation for time remigration has already been theoretically studied and implemented (Jaya et al., 1996; Jaya, 1997), as well as successfully applied to real data from ground-penetrating radar (Jaya, 1997; Jaya et al., 1999). The topic of this paper is the image wave equation for depth remigration. Below, we will briefly review its derivation in 3-D, choose an FD scheme for its implementation, and study its consistency, stability, and convergence. These studies consist of a theoretical investigation as well as numerical testing.

DERIVATION OF THE 3-D IMAGE WAVE EQUATION

As mentioned in the Introduction, the derivation of the image wave equation is based on the kinematic behaviour of the image wavefront, i.e., the reflector image at different migration velocities. Since it has been previously derived by Fomel (1994) and Hubral et al. (1996b) for a two-dimensional medium, we briefly sketch the derivation in three dimensions.

We consider a reflector image Σ_0 to be given that was obtained from a migration of zero-offset data using an incorrect migration velocity, say, v_0. The aim is to construct from Σ_0 the correct reflector image Σ that would have been obtained had the data been migrated using the correct velocity v.

In order to quantitatively understand the kinematics of the "image wave propagation," the input reflector image Σ_0 is considered as a set of points P_0. Each of these points in the input velocity model is kinematically equivalent to a surface in the output velocity model, i.e., both generate the same zero-offset reflection-time surface. The envelope of these equivalent surfaces provides the new reflector image, very much in the same way as a physical wavefront can be thought of as the envelope of Huygens waves that originate at secondary sources along the previous wavefront. Therefore, these equivalent surfaces are referred to as "Huygens image waves" (Hubral et al., 1996b).

Let us now consider a zero-offset experiment with coincident sources and receivers at positions described by coordinates ξ and η on the planar earth surface. Then each of these Huygens image waves is the surface that in the output velocity model v has the same traveltime surface $t(\xi,\eta)$ as the given point $P_0 = (x_0, y_0, z_0)$ in the input velocity model v_0. The traveltime of point P_0 is

$$t(\xi,\eta) = \frac{2}{v_0}\sqrt{(\xi - x_0)^2 + (\eta - y_0)^2 + z_0^2}\ . \tag{1}$$

The Huygens image wave can be constructed as the envelope of the isochrons of all points on this traveltime surface. For a given pair of coordinates ξ and η, the corresponding isochron is the set of points $P = (x, y, z)$ that satisfies

$$\frac{2}{v}\sqrt{(\xi - x)^2 + (\eta - y)^2 + z^2} = t(\xi,\eta)\ . \tag{2}$$

Since the traveltime $t(\xi,\eta)$ in equations (1) and (2) is, by definition, the same, the ensemble of isochrons to this traveltime surface can be described by the function

$$F(\xi,\eta) = \frac{v^2}{v_0^2}\left[(\xi - x_0)^2 + (\eta - y_0)^2 + z_0^2\right] - (\xi - x)^2 - (\eta - y)^2 - z^2 = 0\ , \tag{3}$$

parameterized by the coordinates of the zero-offset data space, ξ and η. To construct the desired Huygens image wave, these parameters must be eliminated by the envelope conditions

$$\frac{\partial F}{\partial \xi} = 0 \qquad \text{and} \qquad \frac{\partial F}{\partial \eta} = 0\ . \tag{4}$$

These conditions yield

$$\xi = \frac{x - m^2 x_0}{1 - m^2} \qquad \text{and} \qquad \eta = \frac{y - m^2 y_0}{1 - m^2}\ , \qquad \text{where} \qquad m = v/v_0\ . \tag{5}$$

Substitution of these results in equation (3) and solution for z yields the following expression for the 3-D Huygens image wave

$$z = m\sqrt{z_0^2 + \frac{1}{1 - m^2}\left[(x - x_0)^2 + (y - y_0)^2\right]}\ . \tag{6}$$

Figure 1 shows a 2-D sketch of the ensemble of isochrons described by equation (3). The envelope formed by all these isochrons is the Huygens image wave described by equation (6). In other words, a reflector of the shape of this envelope would, in a medium with velocity v, create the same zero-offset traveltime surface as point P_0 in a medium with velocity v_0.

Solution of equation (6) for v yields an equation of the form $v = \mathcal{V}(x, y, z)$, where $\mathcal{V}$ is the eikonal of the image wave. For simplicity, we will work with the normalized eikonal $\mathcal{M}(x, y, z) = \mathcal{V}(x, y, z)/v_0$, which

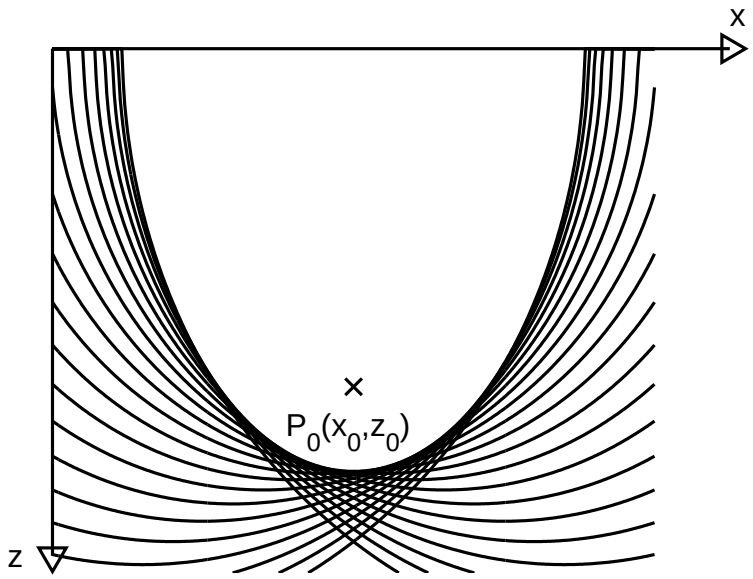

Figure 1: 2-D sketch of the ensemble of isochrons of all points on the traveltime surface in equation (1). Their envelope is the Huygens image wave described by equation (6). The sketch represents a situation where $v > v_0$.

is obtained from solving equation (6) for $m = v/v_0$ instead of v. To find a differential equation for this eikonal, the corresponding expression has to be differentiated with respect to x, y, and z and the derivatives must be combined in such a way that x_0, y_0, and z_0 are eliminated. The resulting differential equation is the eikonal equation for the image wave propagation. However, since equation (6) is a quadratic equation in m, it is easier to substitute directly $m = \mathcal{M}(x, y, z)$ in that equation and differentiate implicitely. Denoting the partial derivatives of $\mathcal{M}$ by $\mathcal{M}_x$, $\mathcal{M}_y$, and $\mathcal{M}_z$, respectively, we can write

$$0 = \mathcal{M}_x \mathcal{X} + \frac{\mathcal{M}^2}{z} \frac{x - x_0}{1 - \mathcal{M}^2} , \tag{7a}$$

$$0 = \mathcal{M}_y \mathcal{X} + \frac{\mathcal{M}^2}{z} \frac{y - y_0}{1 - \mathcal{M}^2} , \tag{7b}$$

$$1 = \mathcal{M}_z \mathcal{X} , \tag{7c}$$

where

$$\mathcal{X} = \left. \frac{\partial z}{\partial m} \right|_{m=\mathcal{M}} = \frac{z}{\mathcal{M}} + \frac{\mathcal{M}^3}{z(1 - \mathcal{M}^2)^2} \left[(x - x_0)^2 + (y - y_0)^2 \right] . \tag{8}$$

Here we have used that, because of equation (6) with $m = \mathcal{M}$,

$$\sqrt{z_0^2 + \frac{1}{1 - \mathcal{M}^2} \left[(x - x_0)^2 + (y - y_0)^2 \right]} = \frac{z}{\mathcal{M}} . \tag{9}$$

Now, we solve equations (7a) and (7b) for $x - x_0$ and $y - y_0$, respectively, and (7c) for $\mathcal{X}$. Substitution of the results in equation (8) results then in the desired image eikonal equation

$$\mathcal{M}_x^2 + \mathcal{M}_y^2 + \mathcal{M}_z^2 - \frac{\mathcal{M}}{z} \mathcal{M}_z = 0 . \tag{10}$$

Remembering that $\mathcal{V}$ is obtained from $\mathcal{M}$ by a simple multiplication with the constant v_0, we see that also $\mathcal{V}$ obeys the same image eikonal equation (10).

The last step is to find a second-order differential equation for the "image wavefield" $p(x, y, z)$ such that a substitution of the ray ansatz

$$p(x, y, z) = p_0(x, y, z) f(v - \mathcal{V}(x, y, z)) \, , \tag{11}$$

yields the above eikonal equation. Here, p_0 is the amplitude of the migrated reflector image, i.e., the image wave, and $f(v)$ is the source wavelet as a function of velocity. The simplest differential equation that fulfills the above requirement is

$$p_{xx} + p_{yy} + p_{zz} + \frac{v}{z} p_{vz} = 0 \, . \tag{12}$$

Note that to arrive at the eikonal equation (10) upon substitution of ray ansatz (11) in equation (12), one needs to substitute v by $\mathcal{V}(x, y, z)$. This substitution is, of course, valid on the image wavefront $v = \mathcal{V}$ itself. However, if the wavelet f in equation (11) is of nonzero duration, points off the wavefront are also involved in the propagation of the image. As we will see in the numerical example, this leads to a stretch of the wavelet in the propagating image.

FINITE DIFFERENCES

We consider a grid of depth points and a discretized velocity axis. The image wavefield at a given grid point $(x, y, z) = (k\Delta x, l\Delta y, m\Delta z)$, as calculated for a certain migration velocity $v = n\Delta v$, is denoted by $p^n_{k,l,m}$. On this grid, we approximate the derivatives in equation (12) by finite differences. For the spatial derivatives, we use fourth-order approximations, i.e.,

$$p_{xx} \approx \frac{1}{12(\Delta x)^2} \left[-p^n_{k+2,l,m} - p^n_{k-2,l,m} + 16(p^n_{k+1,l,m} + p^n_{k-1,l,m}) - 30 p^n_{k,l,m} \right] \tag{13}$$

and corresponding expressions for p_{yy} and p_{zz}. For the mixed derivative, we choose a scheme that is forward in v and z, given by

$$p_{vz} \approx \frac{1}{\Delta v \Delta z} \left[p^{n+1}_{k,l,m+1} - p^{n+1}_{k,l,m} - p^n_{k,l,m+1} + p^n_{k,l,m} \right] . \tag{14}$$

Using these approximations for the derivatives in the image wave equation (12) and isolating $p^{n+1}_{k,l,m+1}$, we find the following FD scheme,

$$\begin{aligned} p^{n+1}_{k,l,m+1} \quad = \quad & -\frac{z_m \Delta v \Delta z}{12 v_n} \left\{ \frac{-p^n_{k+2,l,m} - p^n_{k-2,l,m} + 16(p^n_{k+1,l,m} + p^n_{k-1,l,m}) - 30 p^n_{k,l,m}}{(\Delta x)^2} \right. \\ & + \frac{-p^n_{k,l+2,m} - p^n_{k,l-2,m} + 16(p^n_{k,l+1,m} + p^n_{k,l-1,m}) - 30 p^n_{k,l,m}}{(\Delta y)^2} \\ & \left. + \frac{-p^n_{k,l,m+2} - p^n_{k,l,m-2} + 16(p^n_{k,l,m+1} + p^n_{k,l,m-1}) - 30 p^n_{k,l,m}}{(\Delta z)^2} \right\} \\ & + p^{n+1}_{k,l,m} + p^n_{k,l,m+1} - p^n_{k,l,m} \, . \end{aligned} \tag{15}$$

Here, v_n and z_m are the discretized values at the present level, i.e. $v_n = v_0 + n\Delta v$ and $z_m = m\Delta z$.

The initial condition for the propagation of the image wave is, of course, the original migrated section for the velocity v_0. Since the geophysical problem provides no explicit boundary conditions, we use that the field outside the given target zone of the input section should be zero.

We observe from equation (15) that the computation of the wavefield $p^{n+1}_{k,l,m+1}$ at step $n+1$ at gridpoint $(k, l, m+1)$ requires the knowledge of the wavefield $p^{n+1}_{k,l,m}$ at the same step $n+1$ at gridpoint (k, l, m), in addition to the wavefield at the surrounding gridpoints at the previous step n. This fact makes the FD scheme an implicit one. However, its computation would require the solution of a linear system of equations in each step. Such a procedure would, of course, be expensive to realize, particularly for large migrated sections.

For this reason, we prefer to treat equation (15) as an explicit scheme. This is no major problem as $p^{n+1}_{k.l,m}$ is just the value of the image wavefield at the neighboring gridpoint and has been calculated in the

anterior step in z. However, this way of procedure requires an additional boundary condition to initialize the loop in z. We choose again a homogeneous boundary condition.

In order to actually use the FD scheme (15), its consistency and stability need to be investigated, so as to find conditions for the step size Δv as a function of the medium parameters and the grid intervals Δx, Δy, and Δz. This is done in the next sections.

CONSISTENCY

A finite difference scheme is consistent with the corresponding partial differential equation, if for any smooth function $\phi(x, z, v)$, the difference between the differential operator, $\mathcal{D}$, and the discretized operator, $\mathcal{D}^{\Delta v}_{\Delta x,\Delta y,\Delta z}$, applied to ϕ, tends to zero when Δx, Δy, Δz, and Δv tend to zero (Strikwerda, 1989). In symbols, the scheme is required to guarantee that

$$\mathcal{D}\phi - \mathcal{D}^{\Delta v}_{\Delta x,\Delta y,\Delta z}\phi \;\rightarrow\; 0, \qquad \text{for} \qquad \Delta x, \Delta y, \Delta z, \Delta v \;\rightarrow\; 0. \tag{16}$$

We now apply this concept to the image wave equation (12) and its FD scheme (15). The differential operator applied to a function ϕ is

$$\mathcal{D}\phi = \phi_{xx} + \phi_{yy} + \phi_{zz} + \frac{v}{z}\,\phi_{vz}\ . \tag{17}$$

Application of the discretized operator according to scheme (15) to the same function ϕ yields, under consideration of the truncation errors of the approximations (13) and (14), after some straightforward algebra,

$$\begin{aligned}\mathcal{D}^{\Delta v}_{\Delta x,\Delta y\Delta z}\phi \;\;=\;\; & \phi_{xx} + O(\Delta x^4) + \phi_{yy} + O(\Delta y^4) + \phi_{zz} + O(\Delta z^4) \\ & + \frac{v_n}{z_m}\,\left(\phi_{vz} + O(\Delta z) + O(\Delta v)\right)\ .\end{aligned} \tag{18}$$

The difference of equations (17) and (18) yields

$$\mathcal{D}\phi - \mathcal{D}^{\Delta v}_{\Delta x,\Delta z}\phi = O(\Delta x^4) + O(\Delta y^4) + O(\Delta z) + O(\Delta v)\ . \tag{19}$$

We conclude that

$$\mathcal{D}\phi - \mathcal{D}^{\Delta v}_{\Delta x,\Delta y,\Delta z}\phi \;\rightarrow\; 0, \qquad \text{for} \qquad \Delta x, \Delta y, \Delta z, \Delta v \;\rightarrow\; 0\ . \tag{20}$$

i.e., the FD scheme (15) is unconditionally consistent with the image wave equation (12).

STABILITY

According to Lax's theorem (Thomas, 1995), an FD scheme is convergent, i.e., its solutions converges to the solution of the original differential equation, if it is consistent and stable. To determine the conditions under which the FD scheme (15) is stable, we apply the von Neumann criterion (Strikwerda, 1989; Thomas, 1995), i.e., we substitute the wavefield $p^n_{k,l,m}$ in equation (15) by a generic component of its discrete Fourier transform. This reads

$$p^n_{k,l,m} = \xi^n e^{ik\kappa_x\Delta x} e^{il\kappa_y\Delta y} e^{im\kappa_z\Delta z}\ , \tag{21}$$

where κ_x, κ_y, and κ_z are the components of the wavenumber vector in the x-, y-, and z-directions. According to the von Neumann condition, an FD scheme is stable if $p^n_{k,l,m}$ as expressed in equation (21) does not increase for increasing n. This is guaranteed by a ξ the modulus of which satisfies $|\xi| \leq 1$.

From substitution of the discrete Fourier transform (21) in equation (15) and solution of the resulting equation for ξ, we find the expression

$$\begin{aligned}\xi \;\;=\;\; & \frac{1}{(e^{i\kappa_z\Delta z} - 1)}\left\{\frac{16 z_m}{12 v_n}\frac{\Delta v\Delta z}{(\Delta x)^2}\sin^2\frac{\kappa_x\Delta x}{2}\left[3 + \sin^2\frac{\kappa_x\Delta x}{2}\right]\right. \\ & + \frac{16 z_m}{12 v_n}\frac{\Delta v\Delta z}{(\Delta y)^2}\sin^2\frac{\kappa_y\Delta y}{2}\left[3 + \sin^2\frac{\kappa_x\Delta y}{2}\right] \\ & + \left.\frac{16 z_m}{12 v_n}\frac{\Delta v\Delta z}{(\Delta z)^2}\sin^2\frac{\kappa_z\Delta z}{2}\left[3 + \sin^2\frac{\kappa_z\Delta z}{2}\right]\right\} + 1.\end{aligned} \tag{22}$$

Upon denoting the expression within curly brackets by Λ, equation (22) reduces to

$$\xi = \frac{\Lambda}{(e^{i\kappa_z \Delta z} - 1)} + 1 = \left(1 - \frac{\Lambda}{2}\right) - i\left(\frac{\Lambda}{2}\frac{\cos\frac{\kappa_z\Delta z}{2}}{\sin\frac{\kappa_z\Delta z}{2}}\right). \tag{23}$$

We observe that ξ is not defined if $\sin\frac{\kappa_z\Delta z}{2} = 0$. This is not a real restriction to the stability of scheme (15) since it is not difficult to see from equation (23) that

$$\lim_{\sin(\kappa_z\Delta z/2)\to 0} \xi = 1. \tag{24}$$

This means that scheme (15) will be stable for wavenumbers κ_z for which $\sin(\kappa_z\Delta z/2) = 0$ as long as it is stable for all wavenumbers in its vicinity.

Application of the condition $|\xi| \leq 1$ to equation (23) provides the inequation

$$\Lambda^2\left[\frac{1}{4\sin^2\frac{\kappa_z\Delta z}{2}}\right] - \Lambda \leq 0. \tag{25}$$

Since the coefficient of Λ^2 in equation (25) is always positive, we conclude that Λ must satisfy the condition

$$0 \leq \Lambda \leq 4\sin^2\frac{\kappa_z\Delta z}{2}\ . \tag{26}$$

Thus, the stability condition for the FD scheme (15) reads

$$\begin{aligned} 0 \quad \leq \quad & \frac{z_m}{3v_n}\frac{\Delta v\Delta z}{(\Delta x)^2}\sin^2\frac{\kappa_x\Delta x}{2}\left[3 + \sin^2\frac{\kappa_x\Delta x}{2}\right] \\ & + \frac{z_m}{3v_n}\frac{\Delta v\Delta z}{(\Delta y)^2}\sin^2\frac{\kappa_y\Delta y}{2}\left[3 + \sin^2\frac{\kappa_y\Delta y}{2}\right] \\ & + \frac{z_m}{3v_n}\frac{\Delta v\Delta z}{(\Delta z)^2}\sin^2\frac{\kappa_z\Delta z}{2}\left[3 + \sin^2\frac{\kappa_z\Delta z}{2}\right] \leq \sin^2\frac{\kappa_z\Delta z}{2}. \end{aligned} \tag{27}$$

Equation (27) represents the general stability condition for the FD scheme (15). It is, however, hard to appreciate its meaning. Let us thus investigate it in more detail.

The case $\Lambda = 0$ is not really meaningful since this requires $\sin^2\frac{\kappa_x\Delta x}{2} = \sin^2\frac{\kappa_y\Delta y}{2} = \sin^2\frac{\kappa_z\Delta z}{2} = 0$, which can only be satisfied for certain selected values of the wavenumbers κ_x, κ_y, and κ_z.

Note that equation (27) must be satisfied for all wavenumbers κ_x, κ_y, and κ_z involved in the remigration problem to be solved. This can be a difficult condition to meet. The simplest situation is the case where wavenumbers and grid increments are of the same size, such that $\Delta x = \Delta y = \Delta z$ and $\kappa_x\Delta x \approx \kappa_y\Delta y \approx \kappa_z\Delta z$. In this situation, the above condition can be divided by $\sin^2\frac{\kappa_z\Delta z}{2}$ to yield

$$0 < \frac{4z_{\text{max}}}{3v_{\text{min}}}\frac{\Delta v}{\Delta z} + \frac{4z_{\text{max}}}{3v_{\text{min}}}\frac{\Delta v}{\Delta z} + \frac{4z_{\text{max}}}{3v_{\text{min}}}\frac{\Delta v}{\Delta z} \leq 1 \quad \Longrightarrow \quad \Delta v \leq \frac{1}{4}\frac{v_{\text{min}}}{z_{\text{max}}}\Delta z, \tag{28}$$

where we have used that $3 + \sin^2\frac{\kappa_z\Delta z}{2} \leq 4$. Moreover, we have replaced z_m and v_n by their maximum and minimum values, z_{max} and v_{min}, respectively.

If different wavenumbers are involved in different directions, the presence of the term $\sin^2\frac{\kappa_z\Delta z}{2}$ on the right-hand side of equation (27) has an important consequence for the stability of the FD scheme (15). If there are vertical wavenumbers κ_z present in the data for which this term is very close to zero, it will be very hard to make the scheme stable. Very small values of Δv might be needed to fulfill the requirements. We will further comment on this observation below when discussing the numerical examples.

Finally, let us comment on the requirement $\Lambda > 0$. It means that for possitive Δz, only positive values for Δv are admitted. In other words, scheme (15) *can only* be used to propagate a reflector image from smaller to larger velocities. For the inverse direction, a different FD scheme is needed. One can use, e.g., a

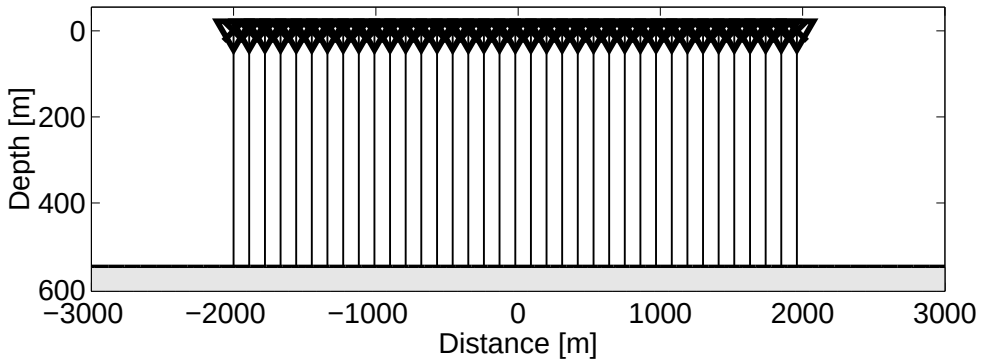

Figure 2: Earth model for the remigration example. Also shown is a family of zero-offset rays.

scheme that is forward in v and backward in z, i.e., one which represents the mixed derivative in equation (12) as

$$p_{vz} = \frac{1}{\Delta v \Delta z}\left[p^{n+1}_{k,l,m} - p^{n+1}_{k,l,m-1} - p^{n}_{k,l,m} + p^{n}_{k.l,m-1}\right]. \tag{29}$$

The stability condition for the corresponding FD scheme is given by equation (27) multiplied by minus one. Therefore, this scheme requires a negative Δv, i.e., it allows only for image propagation from larger to smaller velocities. Other FD schemes are currently under investigation.

NUMERICAL TESTS

In this section, we demonstrate the numerical realization of a remigration by means of the application of FD scheme (15). Because of computational limitations, the numerical testing had to be restricted to the corresponding 2-D scheme, which is obtained from equation (15) by eliminating the second line (i.e., the y-derivative). For the remigration, we used migrated data from a simple earth model (see Figure 2). It consists of two homogeneous halfspaces, separated by a horizontal reflector at a depth of 550 m. The velocities above and below the reflector are $c_1 = 3$ km/s and $c_2 = 3.5$ km/s. The simulated seismic survey is a zero-offset experiment with 401 source-receiver pairs, located at every 10 m between -2000 m and 2000 m along the x-axis.

The input data to the remigration where generated by migrating the so-obtained zero-offset data to depth with a wrong migration velocity of $v_0 = 2$ km/s. The result of this depth migration is depicted in Figure 3a. As we can see, the reflector is imaged at a wrong depth of about 370 m, because of the wrong migration velocity. Note that the target region for migration was chosen quite large so as to include all boundary effects from migration but to eliminate additional boundary reflections from the image wave propagation. For the same reason, the depth axis was extended to $z_{\max} = 1.6$ km.

This wrongly migrated depth section was then remigrated using FD scheme (15). The grid size of the depth region was $\Delta x = \Delta z = 10$ m. According to the 2-D version of stability condition (28) (where the factor $1/4$ is replaced by $3/8$), this implies the use of a velocity increment smaller than $\frac{3}{8}\frac{2}{1.6}10 \approx 4.7$ m/s. We have chosen $\Delta v = 4$ m/s. Parts b and c of Figure 3 show two snapshots of this image wave propagation for velocities $v = 2.4$ km/s and $v = 3$ km/s, the latter being the true medium velocity. We observe that the reflector image in Figure 3c is remigrated to the correct depth of 550 m.

However, there are quite large regions of the remigrated image where the image is obscured by noise. In fact, the noise is many orders of magnitude larger than the actual image. Therefore, to enable the presentation of Figure 3, the error had to be zeroed out wherever it exceeds the amplitude of the reflector image. In this way, one can see the borders of the regions that are affected by the very large error.

What happened in this part of the image? Why is there so large numerical noise, although stability condition (28) is satisfied? The reason is a violation of the stricter condition (27). Looking at the wrongly migrated reflector image in Figure 3, we see that at the reflector image itself, the wavenumber content in the horizontal direction is rather low. This means that $\sin^2 \frac{\kappa_x \Delta x}{2}$ is a very small quantity in equation (27). Therefore, the scheme (15) is stable as long as condition (28) is satisfied. At the tips of the migration

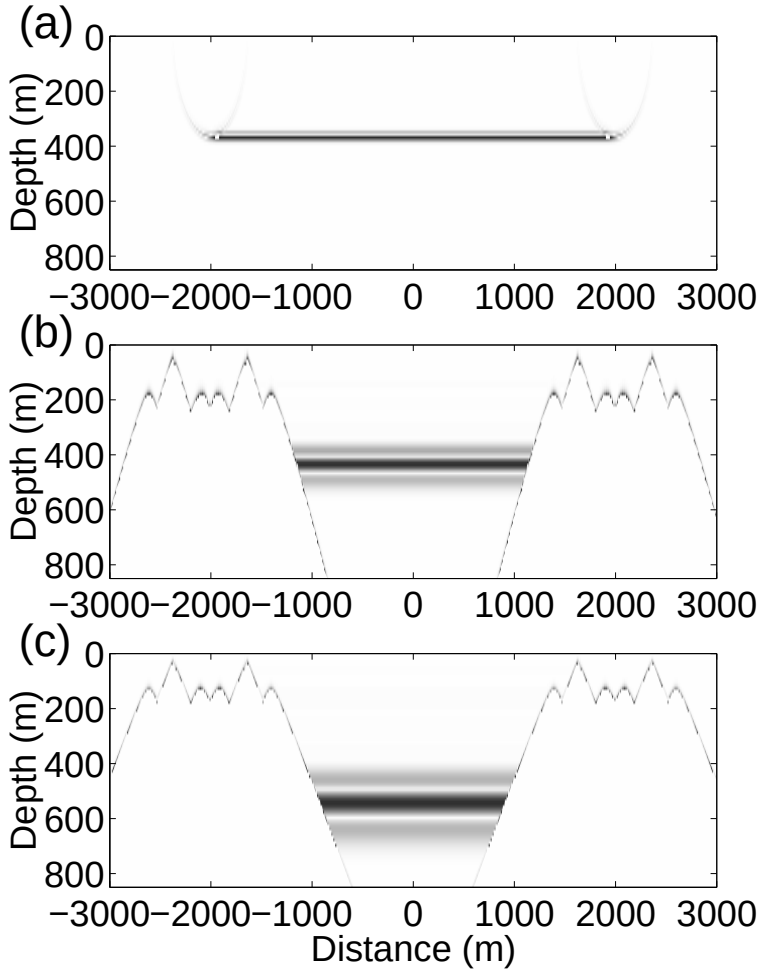

Figure 3: Image wave propagation. Direct implementation. (a) Input data for the remigration example: data after migration with a wrong migration velocity of $v_0 = 2$ km/s. (b) Remigrated image for $v = 2.4$ km/s. (c) Remigrated image for $v = 3$ km/s.

boundary effects (smiles), however, we have higher wavenumbers in the horizontal than in the vertical direction. As commented before, this gives rise to a violation of condition (27). This causes the numerical error.

The fact that the numerical error indeed originates at the tips of the boundary effect is illustrated in Figure 4. It shows the image wave propagation at a very early stage for a migration velocity of $v = 2.04$ km/s.

There is, however, a way to obtain a better remigration result with scheme (15). Figure 5 depicts the results of an FD remigration using scheme (15) in reverse implementation. In other words, while Figure 3 represents the results of the FD scheme exactly in the way it is written in equation (15), the results in Figure 5 where obtained by solving equation (15) for $p^{n+1}_{k,l,m}$. In this way, $p^{n+1}_{k,l,m}$ is calculated at the mth level in z as a function of $p^{n+1}_{k,l,m+1}$ at the $(m+1)$th level, together with the terms of step n.

Why are the two results of Figures 3 and 5 are different, although they are obtained from implementations of the same FD scheme and are thus governed by the same stability conditions? The reason is that the numerical error caused by the unstability affects the direct and reverse implementations in different ways. Because of the factor z that multiplies the spatial difference terms in scheme (15), this error increases exponentially in the direct implementation, which is realized in the direction of increasing z. On the other hand, it is damped in the reverse implementation, which is realized in the direction of decreasing z.

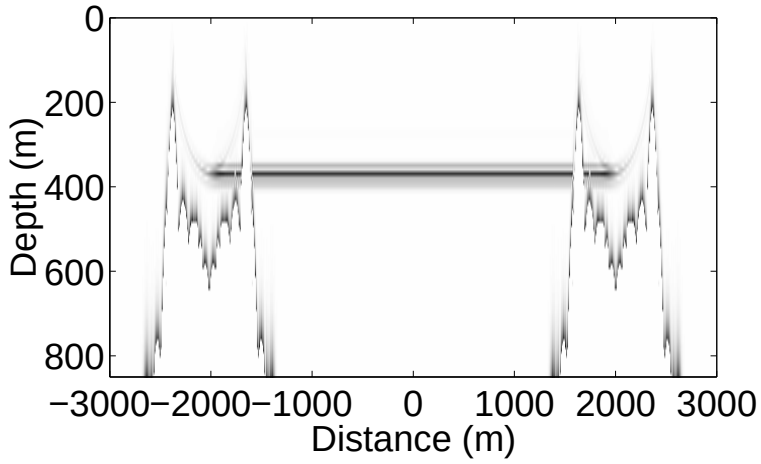

Figure 4: Snapshot of image wave propagation with the direct implementation of scheme (15) at $v = 2.04$ km/s. The numerical error originates at the tips of the boundary effect.

As a final observation, let us comment on the pulse stretch that can be seen in both, Figures 3 and 5. Note that the source pulse that represents the reflector image in Figure 5c is much longer than in Figure 5a. This effect has two reasons. The first one is the conventional pulse stretch due to depth migration, which is proportional to the migration velocity (Tygel et al., 1994). Since the migration velocity has increased from 2 km/s to 3 km/s, this implies a 1.5 times longer wavelet. However, the stretch that can be seen in Figure 5 is much larger than that. The second reason that causes the additional stretch is the substitution of $\mathcal{V}$ by v in the derivation of the image wave equation (12). This means that off the reflector, a slight error is introduced into the kinematic behavior of the pulse. In effect, this causes the upper part of the pulse to be moved to shallower depths than it should be, while at the same time the lower part of the pulse is moved to greater depths.

CONCLUSIONS

The image wave equation for depth remigration is a second-order partial differential equation that describes the "propagation" of a migrated reflector image as a function of a changing migration velocity (Hubral et al., 1996b). In this paper, we have studied the consistency and stability of an FD scheme for this equation. The theoretical stability condition obtained from the von Neumann criterion points towards general difficulties of the process when remigrating data containing large wavenumbers in the horizontal directions. Numerical tests have demonstrated that instabilities indeed arise in such situations. They can, however, be controlled by using an implementation of the FD scheme in the reverse vertical direction.

With the investigated FD schemes, reflector images can be remigrated only either to larger or to smaller migration velocities. The scheme forward in v and forward in z allows only for an increase, the scheme forward in v and backward in z only for a decrease of the migration velocity. Other FD schemes that may be less restrictive are currently under investigation.

The remigrated images present an exaggerated pulse strech. This is a drawback of image wave remigration as it degrades the vertical resolution of the remigrated image. The effect is inherent to the method as it is introduced by the very image wave equation that describes the propagation. Further investigations are necessary to evaluate whether this effect can be reduced by a modification of the image wave equation.

ACKNOWLEDGEMENTS

This work was kindly supported by the sponsors of the *Wave Inversion Technology (WIT) Consortium*, Karlsruhe, Germany.

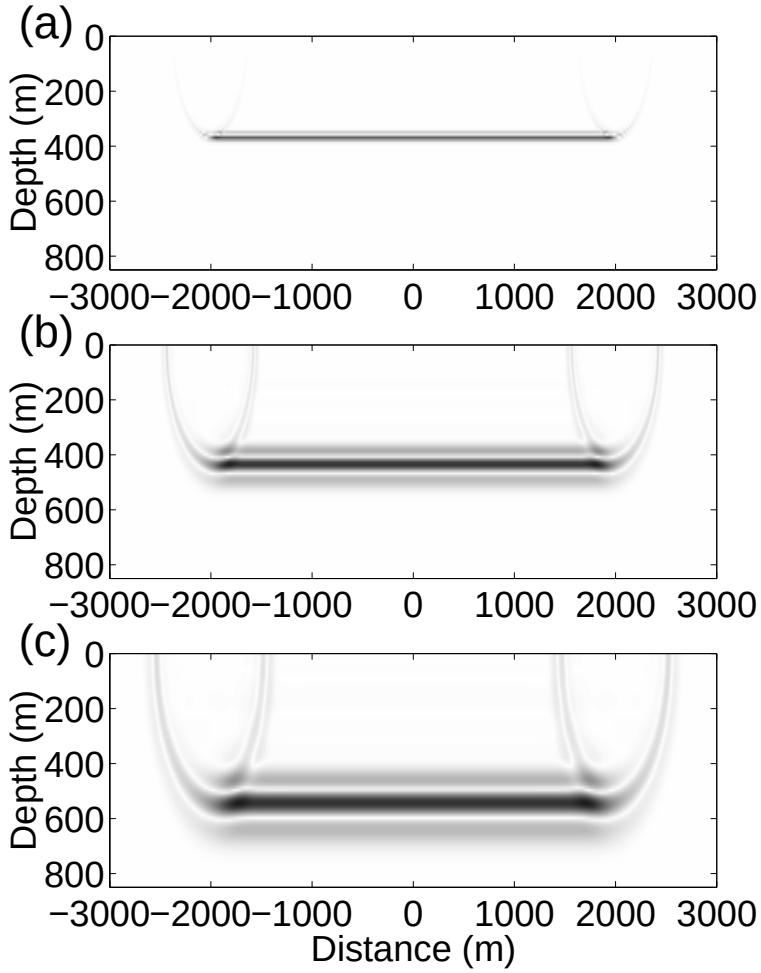

Figure 5: Image wave propagation. Reverse implementation. (a) Input data for the remigration example: data after migration with a wrong migration velocity of $v_0 = 2$ km/s. (b) Remigrated image for $v = 2.4$ km/s. (c) Remigrated image for $v = 3$ km/s.

REFERENCES

Fomel, S. (1994). Method of velocity continuation in the problem of seismic time migration. *Russian Geology and Geophysics*, 35(5):100–111.

Hubral, P., Schleicher, J., and Tygel, M. (1996a). A unified approach to 3-D seismic reflection imaging – Part I: Basic concepts. *Geophysics*, 61(3):742–758.

Hubral, P., Tygel, M., and Schleicher, J. (1996b). Seismic image waves. *Geophys. J. Internat.*, 125(2):431–442.

Jaya, M. (1997). *Imaging reflection seismic data using the method of velocity continuation*. Dissertation, Universität Karlsruhe (TH).

Jaya, M., Botelho, M., Hubral, P., and Liebhardt, G. (1999). Remigration of ground-penetrating radar data. *J. Appl. Geoph.*, 41:19–30.

Jaya, M., Schleicher, J., and Hubral, P. (1996). Post-stack time-domain remigration. In *Abstracts*, page X017, Amsterdam. Europ. Assn. Geosc. Eng.

Rothman, D., Levin, S., and Rocca, F. (1985). Residual migration: Applications and limitations. *Geophysics*, 50(1):110–126.

Strikwerda, J. (1989). *Finite Difference Schemes and Partial Differential Equations*. Wadsworth & Brooks, California.

Thomas, J. (1995). *Numerical Partial Differential Equations*. Springer-Verlag, New York.

Tygel, M., Schleicher, J., and Hubral, P. (1994). Pulse distortion in depth migration. *Geophysics*, 59(10):1561–1569.

Tygel, M., Schleicher, J., and Hubral, P. (1998). Image waves. In *Proceedings, Internat. Conf. on Electro-Magnetic Theory, Internat. Union of Radio Science, Thessaloniki*, pages 760–762.